Grade: 97%

Scintillation Detectors

1. Abstract

Gamma spectroscopy was conducted using a typical sodium iodide (NaI(Tl)) scintillation detector. NaI(Tl) was chosen in this experiment because it is an inorganic scintillator, making it effective in detecting gamma-rays. Spectrums of known radioactive sources were taken, and their resulting pulses were investigated. The expected gamma-ray energies emitted by the sources used were known, so the outputted signals were compared in order to determine the relationship between the spectrum's output and the actual energies being emitted. A linear regression was conducted for this data and showed that the correlation between the average peak channel number and the actual gamma-ray energy were extremely strong, with a resulting R^2 value of 0.99. This linear regression allowed further spectrums to be converted from channel number to energy, allowing for further investigations, such as a background analysis, where the cause of outputted peaks in a spectrum was not necessarily known to begin with. The NaI(Tl) detector was also used while changing the shaping time of the amplifier. This was done with and without the outputted signal traveling through a preamplifier in order to determine the effect the shaping time had on the resulting pulse. It was concluded that the shaping time does not affect the outputted peaks when a preamplifier is used, but without the preamplifier, the outputted peaks decrease in channel number as the shaping time increases. The relationship between the applied voltage to the PMT and the average channel peak number (output voltage) was determined as well. A linear regression was performed and this trend was used to determine the gain of the PMT being used. The gain was calculated to be $1.39 \pm 0.24 * 10^{-6}$ which agreed fairly closely to the PMT's manufacturer specifications.

Finally, an organic scintillator was used to demonstrate the differences between the two types of scintillation detectors. Spectrums were taken for known sources to demonstrate the lack of full energy peaks outputted with an organic detector, due to its inability to accurately detect gamma-

rays. The data analysis conducted in this report shows the experiment was carried out properly, as results align with incoming expectations for the uses and functions of scintillation detectors.

2. Introduction

Many radioactive materials can be distinguished from the detection of their emitted gamma-rays. Different elements emit gamma-rays at differing energies, so the ability to detect and distinguish between gamma-rays is a useful tool in any field dealing with radiation. Gamma spectroscopy refers to this practice of analyzing these differing gamma-rays on an energy spectrum. To begin however, one must first be able to detect the radioactive photons. Scintillation detectors are commonly used in gamma spectroscopy for their ability to accurately detect gamma-rays at varying energies. A scintillator can be composed of solid, liquid or gas materials. When ionizing radiation passes through these materials, scintillations of visible light photons are produced. These visible photons will then be collected to produce an electronic signal, which will allow for the detection of the radiation.

Before discussing how the visible photons are measured, it must first be understood how exactly they are produced. The production of these photons depends on what type of scintillation detector being used. For the purposes of this experiment we will be investigating the two major types of scintillators, organic and inorganic. As stated previously, scintillators can be made up of differing materials, and this difference in make-up is the distinguishing factor between organic and inorganic scintillators.

Organic scintillators are comprised of polymerized plastics or liquids and characterized by the benzene rings in there material structure [1]. For organic scintillators, the mechanism which produces the visible photons revolves around the molecular makeup of scintillator. When the incident radiation strikes the scintillator, it excites the electrons from their resting ground state, to a higher energy level. Once they are excited, they will begin to fall back down to the ground state of lower energy. This excitation from the ground state, and then return produces a visible photon. If this photon carries enough energy to not be reabsorbed by the material, it will escape and be able to be collected for detection [2].

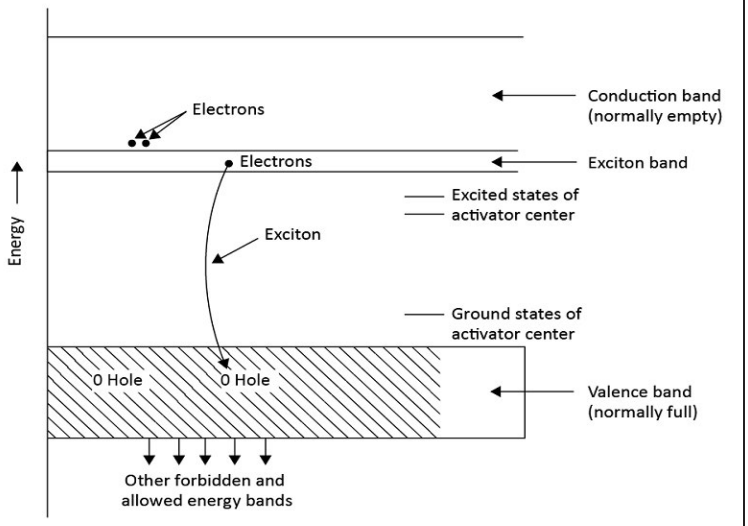

Figure 1: Energy bands of an inorganic scintillation crystal [3]

Inorganic scintillators differ in composition from organic scintillators as they are comprised of solid crystalline structures. Within this crystalline structure is the addition to what is known as an "activator". This "activator" is the important component that allows the emission of photons to take place. When the incident ionizing radiation strikes the crystal, electrons are excited and are raised to the conduction band, leaving behind holes where they used to be in the valence band (Figure 1). The electron, the hole, or both can be captured by the activator in the scintillator, leaving it in an excited state. As the excited state returns to the ground state, a photon is emitted [4]. One of the most common inorganic scintillators is comprised of sodium iodide and activated with thallium (NaI(Tl)). This was the inorganic scintillator used for the collection of the majority of this report.

There are different advantages and disadvantages associated with both types of detectors. These need to be fully understood to ensure the best detector is being used for the given laboratory situation. Inorganic scintillators produce better light outputs and have a better energy resolution, but they also have a slower response time when compared to organic scintillators. This makes organic scintillators better for fast timing experiments. Along with response time, organic scintillators have the advantage that they can be constructed and molded into different shapes, which is advantageous in some instances. A drawback however is organic scintillators lower energy resolution and inability to detect full energy peaks of gamma-rays.

Once the visible photons have escaped the scintillator, they must now be properly collected in order to detect the radiation. This is done using a Photomultiplier Tube (PMT). The job of the PMT is directly in the name, to multiply the visible photons. When radiation passes through the scintillator, the resulting photons that emitted are very faint. They must be multiplied in order to

produce a strong enough signal that will be able to be distinguishable. The PMT is comprised of three main elements, the photocathode, a series of dynodes, and finally the anode (Figure 2).

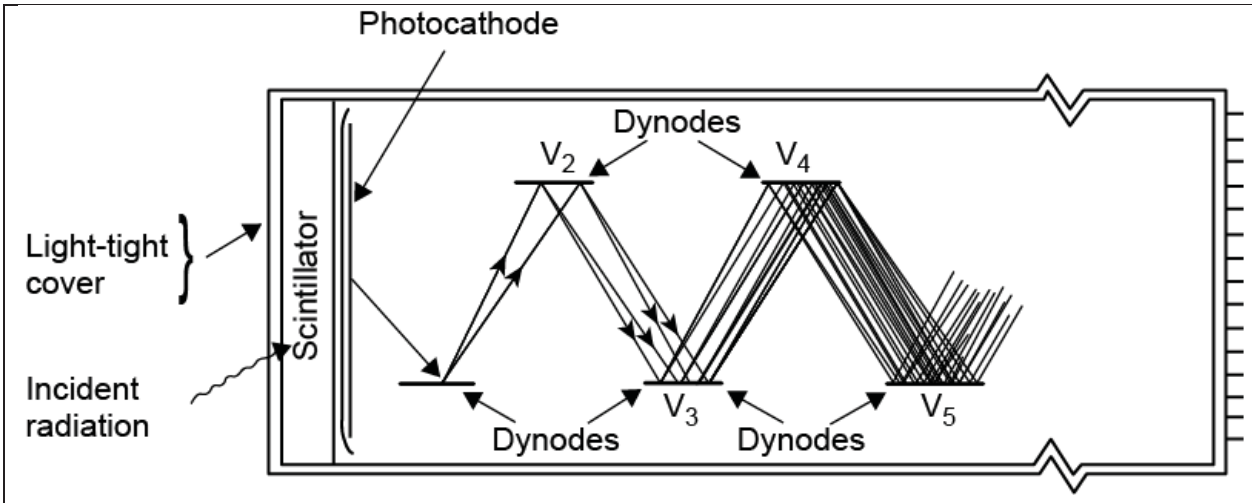

Figure 2: Photomultiplier Tube Diagram [3]

The photocathode is the first step in the PMT. As the visible photons are emitted they are directed through the photocathode. It is here where the visible photons are converted into electrons. This is done through the photoelectric effect [5]. Now that the light has been converted into electrons, they will next be multiplied down the PMT through a series of dynodes before electrons reach the anode and produce a signal.

The amount of dynodes in the PMT and their configuration can vary depending on the make and model of the PMT. For the purpose of understanding, a more linear series of dynodes will be investigated. After leaving the photocathode, the electrons are directed to the first dynode through an applied voltage. Once the electrons reach the first dynode, they are multiplied and directed to the second dynode. This pattern continues and each time the electrons strike the next dynode in the series, more electrons are released. One can see how the electrons which first strike the first dynode, are then multiplied by the time they reach the last dynode.

Once the electrons have been multiplied down the series of dynodes, they are collected at the positively charged anode. This is where the electronic signal is produced from the initial ionizing radiation incident on the scintillator.

For the purposes of the data collection and further data analysis, this general understanding of the geometry and functionality of each step of the scintillation detector was needed.

Along with the understanding of the physical characteristics and functions of the scintillation detectors, an understanding of the resulting signal is needed in order to accurately interpret the resulting spectrum that was recorded. A general box diagram has been included in Figure 3. The main components are the preamplifier, amplifier, and the single or multi-channel analyzer.

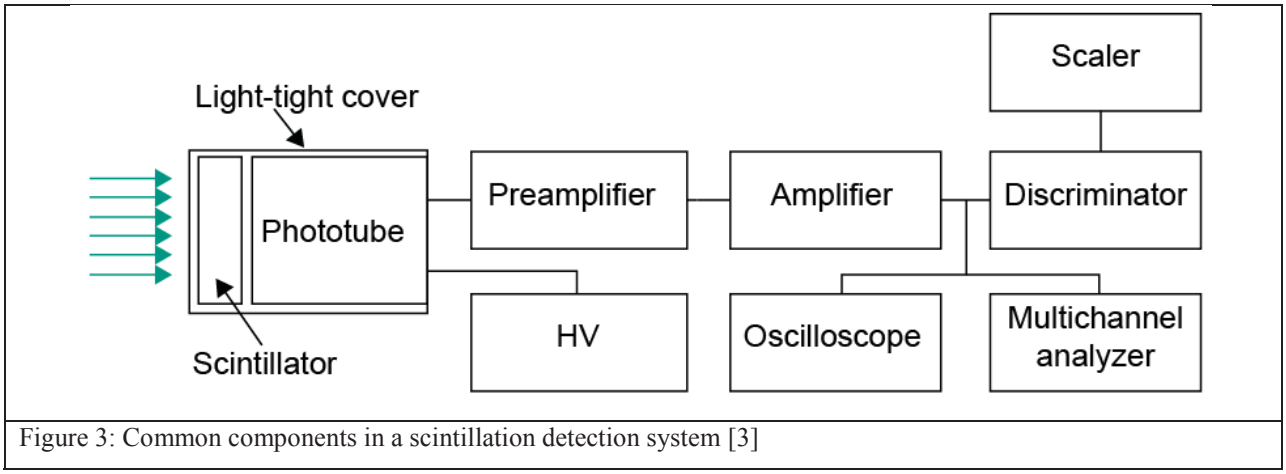

Figure 3: Common components in a scintillation detection system [3]

When the signal leaves the PMT, it must be amplified in order to easily distinguish it as a pulse and not outside sources of radiation. This amplification is done through the amplifier, which can either receive the signal directly from the PMT, or receive the signal after it passes through a preamplifier. In this experiment this difference in configuration, with or without a preamplifier, will be investigated to determine its effects.

The main purpose of the preamplifier is to provide the best coupling between the PMT and the rest of the counting system, as well as minimize the noise so that only the desired signal is reaching the amplifier. Once at the amplifier, the signal is both amplified and shaped to make the desired signal easier to distinguish and analyze [6].

Next the amplified pulse is sent through either a single-channel analyzer (SCA) or a multi-channel analyzer (MCA). The difference between the two is how the signal pulse is recorded. For a SCA the voltage pulse is counted for a specified range. A MCA on the other hand, separates the various voltage pulses into different channels depending on their height. This

results in a full spectrum of the energy distribution [3]. This full energy spectrum is what is desired for this experiment so the signal will pass through a MCA.

For the purposes of this analysis, gamma-ray spectroscopy will be conducted to further understand both inorganic and organic scintillation detectors. With a general understanding of the detectors geometries, functions, and resulting pulse signal paths, proper analysis and conclusions should be able to be made, as well as comparisons of collected data to the expected theoretical trends.

3. Experimental

To begin the experiment, the laboratory instructor performed a demonstration of the assembly of a scintillator detector. A Hammamatsu H6533 1" PMT was properly cleaned off before being coated with a small amount of silicone optical coupling grease. A 1x1 inch NaI (Tl) scintillation crystal was then placed on the PMT and turned clockwise to eliminate air pockets in the coupling grease, before the PMT and scintillator were firmly tapped along their edges with electrical tape.

This assembled NaI(Tl) detector and was connected to high voltage power supply had it's PMT output connected to a Cremate 150 Cr-133 preamplifier which then was connected to an ORTEC 572A amplifier which was finally connected to an ORTEC 927 MCA. ORTEC Maestro Acquisition Software was used to display the signal throughout the experiments.

With an applied voltage to the PMT set to -900V and a conversion gain and acquisition time of the ORTEC Maestro Acquisition Software set to 1024 and 30 second, a spectrum was taken for a Cs-137 source using the assembled NaI(Tl) detector. The effects of the applied voltage to the PMT was investigated by repeating this spectrum four more times with the applied voltage ranging between -975V and -1325V. The resulting peak channels were determined for each spectrum and analyzed to determine the relationship between the applied voltage and outputted spectra voltage.

With the applied voltage then held constant, the ORTEC 572A amplifier's shaping times were investigated by taking spectrums of the same Cs-137 source used above at all available shaping times. The resulting energy peak channels were compared to one another to determine the effect of the amplifier's shaping time on the energy spectrum. This was repeated, but this time the

signal bypassed the Cr-113 preamplifier and went directly from the PMT to the ORTEC 572A amplifier. As before the resulting spectrums were compared against themselves, as well as to the spectrums that used the preamplifier to further investigate the spectral effects of the amplifier's change in shaping time.

The NaI(Tl) detector was replaced by an assembled organic scintillation detector. The organic scintillator's performance was investigated by taking 5 different spectrums; each using a different gamma-ray source (Cs-137, Co-57, Na-22, Mn-54, and Cd-109). The resulting spectrums were saved and compared to one another. Along with visual comparisons, the properly weighted areas under each spectrums were determined and compared to one another to investigate the functionality of the assembled organic scintillator being used.

The assembled organic scintillation detector was replaced by a preassembled Canberra/ORTEC NaI(Tl) Detector. To begin, short acquisitions were taken with Maestro for a Cs-137 button source to calibrate the detector. All of the button sources were then locked away in the laboratory safe and a 20-minute background spectrum was taken and saved. This will be used to investigate background conditions, and compared with future source spectrums to distinguish source caused peaks from background peaks.

The preassembled NaI(Tl) detector was next used to collect five spectrums for 5 different button sources (Cs-137, Co-57, Na-22, Co-60, and Cd-109). Each of the spectrums output peak channels were investigated. A linear regression was found for the outputted peaks and their know gamma-ray energies to investigate the linearity of the detector. These spectrums will also be used to investigate the detectors total efficiency as well as energy resolution.

The NaI(Tl) detector was then disconnected from the MCA and connected to the ORTEC SCA. An integral pulse height spectrum was compiled by taking 30 sec counts of a Cs-137 source by increasing the LLD setting in increments of 0.25 V. This was done until the counts recorded neared zero. This integral pulse height spectrum will be compared against a differential spectrum conducted earlier in the lab to investigate their differences.

4. Results

Five spectrums were taken for the Cs-137 source with the applied voltage ranging from -975 V to -1225 V (Table 1). The average channel number of the full energy peak was determined for each spectrum, along with its uncertainty. The full energy peak was singled out and the counts recorded in each channel were multiplied by the channel number in which they were recorded. The average channel number ($\bar{x}$) and standard deviation (σ_{x_i}) and standard deviation of the mean were then calculated using the following two equations (Where N = total number of channels in the region being investigated).

$$\bar{x} = \frac{Sum\ of\ the\ Channel\ \#*Counts\ in\ Channel}{Sum\ of\ Counts} \quad (1)$$

$$\sigma_{x_i} = \sqrt{\frac{\sum(x_i - \bar{x})^2}{N-1}} \quad (2)$$

$$\sigma_{\bar{x}} = \frac{\sigma_{x_i}}{\sqrt{N}} \quad (3)$$

Table 1: Average peak channel numbers for Cs-137 source at differing applied voltages

Applied Voltage (V)	Average Peak Channel Number	ln(Applied Voltage)	ln(Average Peak Channel #)
976	174 ± 2	2.989	2.241
1101	406 ± 3	3.042	2.608
1049	289 ± 3	3.021	2.461
1201	742 ± 4	3.080	2.870
1225	845 ± 4	3.088	2.927

The natural log was taken for both the applied voltage and the average channel number and then plotted against one another (Figure 4). A liner regression was conducted and the equation as well as the correlation coefficient (R^2) have been included.

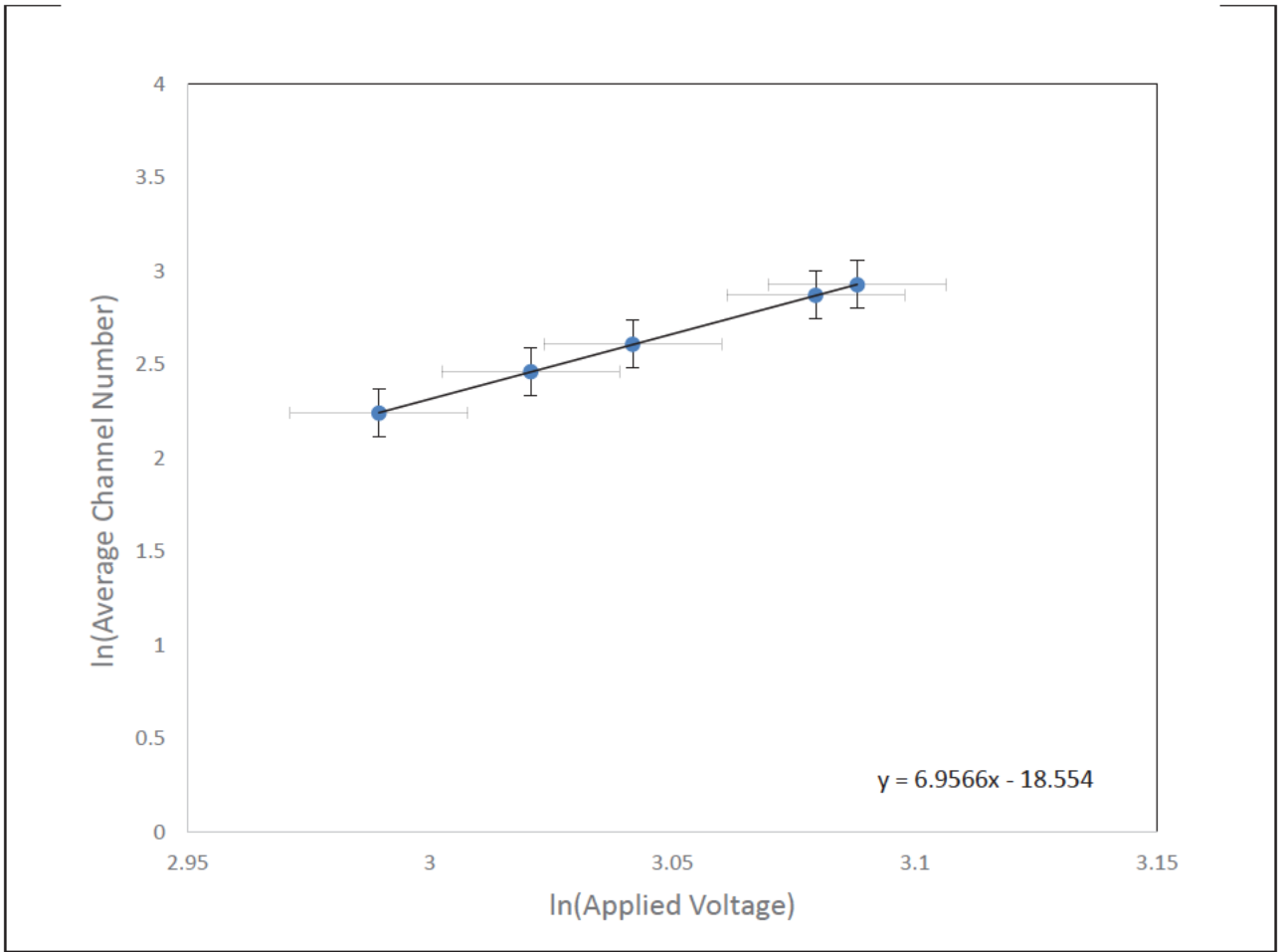

Figure 4: The natural log of the applied voltage versus the natural log of full energy peak average channel number (Error bars included)

The gain of the PMT is found using the following equation.

$$G = (A * V^n)^N \tag{4}$$

N represents the number of dynodes, and V represents the applied voltage between each dynode. The technical specifications for our PMT (Hammamatsu H6533 1' PMT) state that the PMT has 10 dynodes [6]. There was 1100 V being applied so the voltage between each dynode would be 110V (1100V/10 dynodes).

When you take the natural log of both sides of equation 4 above, you get a resulting function of:

$$\ln(G) = Nn\ln(V) + N\ln(A) \tag{5}$$

When compared to the general function of $y = mx + b$ which was found and stated in Figure 4, one can see that the ln(V) = x in this case so the slope $m = Nn$ and the y-intercept $b = Nln(A)$. These two equations were used with the slope and y-intercept stated in Figure 4 to determine the values of A and n (A = 0.15639 and n = 0.69566). These values were then plugged back into equation 4 to determine the gain of the PMT was $1.39 \pm 0.24 * 10^{-6}$.

The manufacture's specifications for the Hammamatsu H6533 states that the gain of the PMT is $5.7 * 10^{-6}$ [6]. Although the determined gain is off from the gain calculated, it is still on the same order of magnitude. Also, the technical specifications are trying to promote the PMT and its functions so it would make sense for the manufacturer would put the highest gain possible. Although this might not be wrong, it might be an inflated term so the gain of $1.39 \pm 0.24 * 10^{-6}$ could be closer to the actual technical specification then originally though.

With the applied voltage held constant at -1100V, a spectrum of the Cs-137 source was analyzed for all available shaping times (0.5μs - 10 μs). The average channel number of the full energy peak was determined as before and included in Table 2.

Table 2: Average channel number with changes in shaping time

Shaping Time (μs)	Average Channel Number (With Preamplifier)	Average Channel Number (Bypassing Preamplifier)
0.5	398 ± 3	666 ± 3
1	426 ± 3	445 ± 3
2	449 ± 3	261 ± 2
3	435 ± 3	178.9 ± 1.9
6	409 ± 3	88.9 ± 1.5
10	394 ± 3	53.2 ± 1.2

This portion of the experiment was conducted twice, once with the signal from the PMT passing through both the preamplifier and the amplifier, and again with the signal bypassing the amplifier. The shaping time versus the average channel number have been plotted against each other for both cases (Figure 5) as well as a comparison of the spectrums at the smallest and largest shaping time (Figure 6).

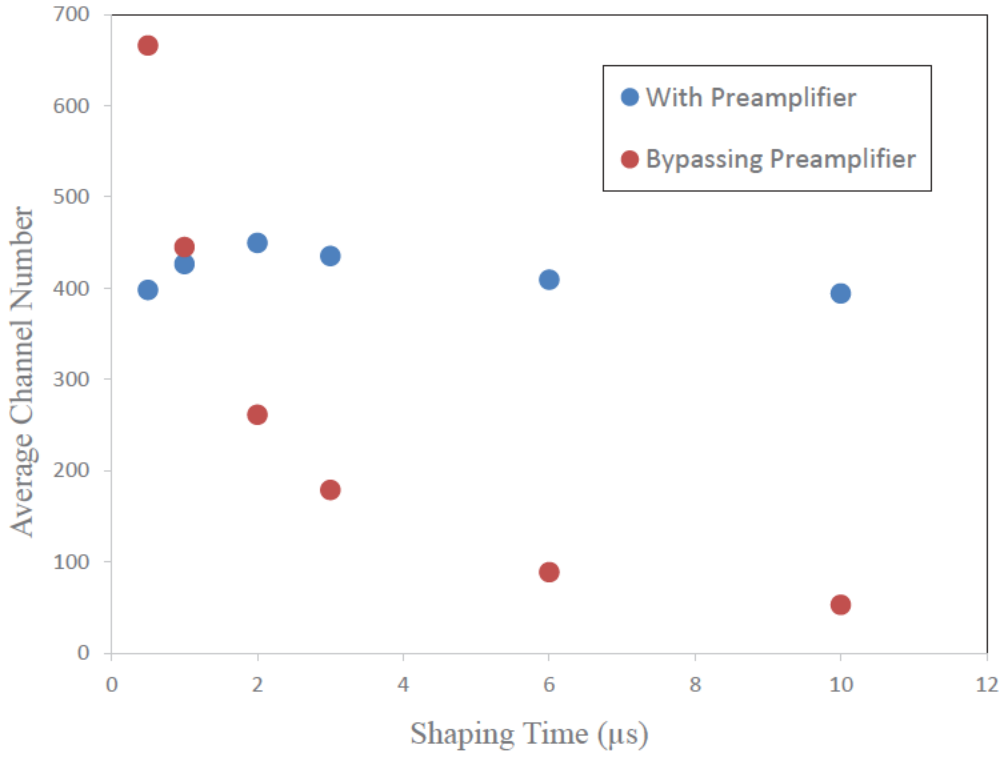

Figure 5: Average channel number versus shaping time with, and without signal going through a preamplifier (Note: Error bars have not been included because they are unable to be seen)

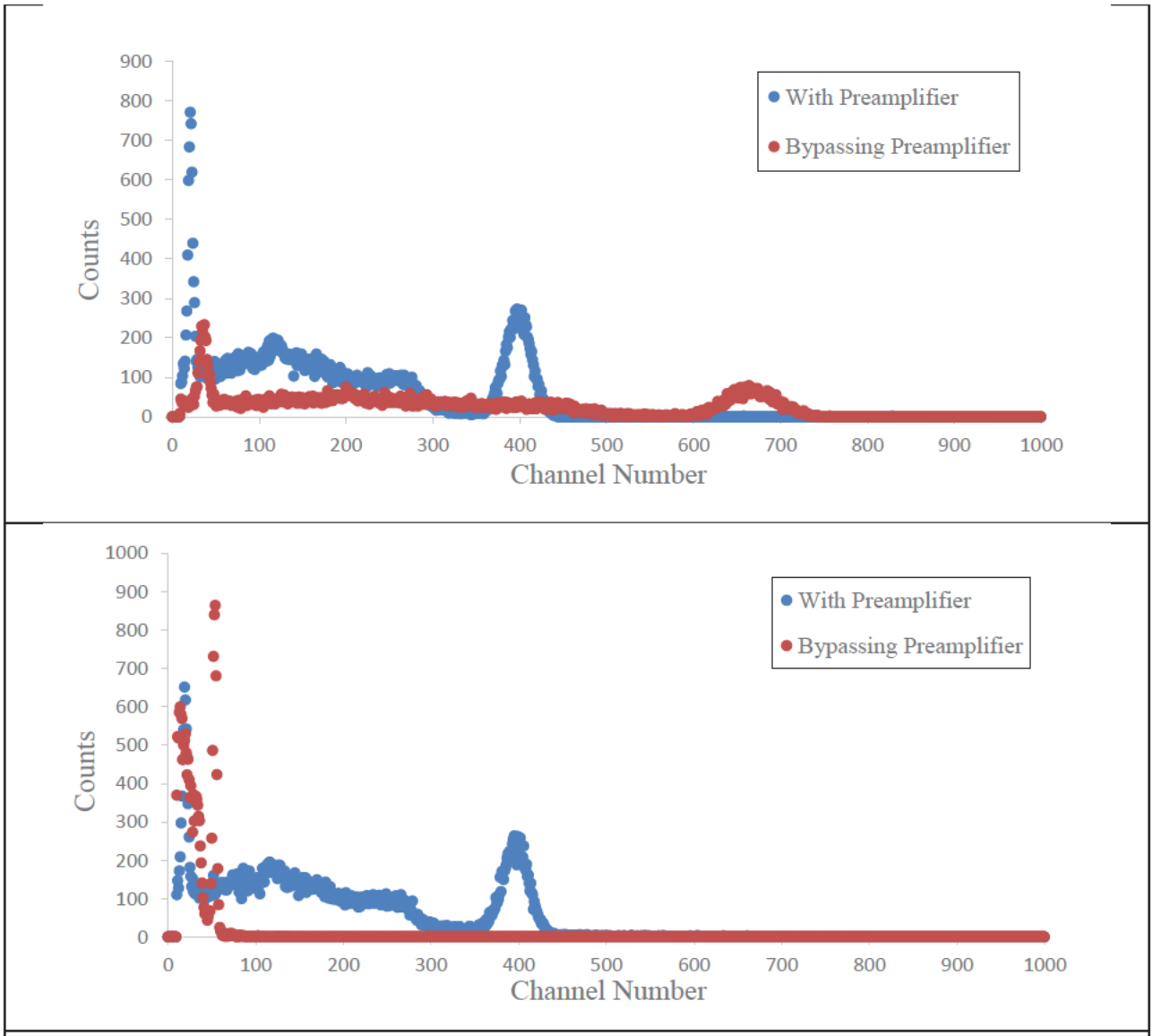

Figure 6: Top: Full energy spectrum of Cs-137 at shaping time of 0.5 μs with, and without the signal passing through preamplifier. Bottom: Full energy spectrum of Cs-137 at shaping time of 10 μs with, and without the signal passing through preamplifier.

As one can see from Figure 5, when the signal from the PMT passes through the preamplifier before going through the amplifier, the difference in shaping time does not seem to impact the resulting signal's peak average channel number. This however is not the case when the preamplifier is bypassed, as the signal's peak average channel decreases exponentially as the shaping time increases. This trend can also be seen in the full energy spectrums plotted in Figure 6. When the signal is passed through the preamplifier, the energy peak (seen above around channel 400) does not change with respect to the increase in shaping time, but without the preamplifier, the signal peak channel number is greatly decreased as the shaping time increases

(seen above around channel 660 for 0.5 µs and down below channel 100 for 10 µs). The preamplifier plays a major part in preventing noise from reaching the amplifier. This could be the cause of the drastic change in outputted energy when the preamplifier is bypassed.

An organic scintillator detector was used for each of the sources listed in Table 3. The spectrums have each been plotted on the same chart as seen in Figure 7.

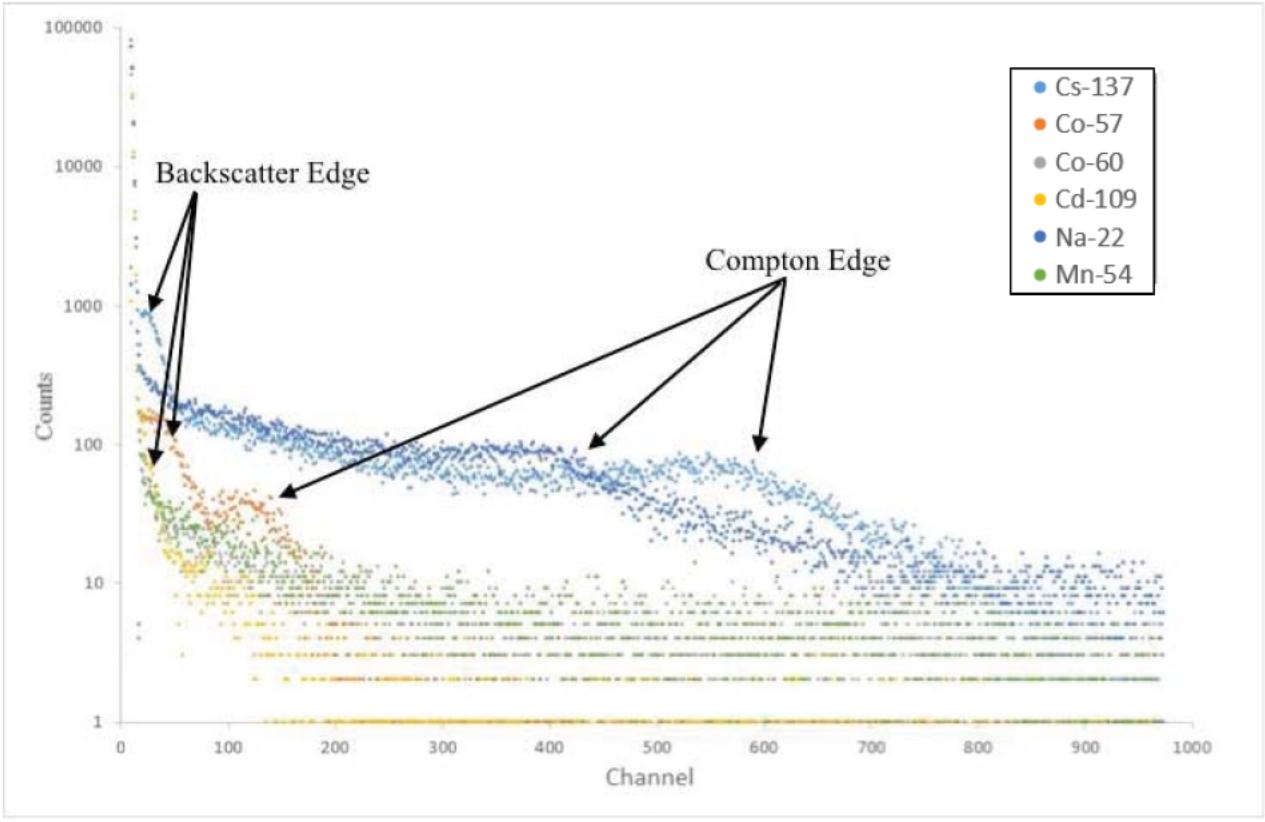

Figure 7: Organic scintillator detector spectrums (Note, y-axis is a logarithmic scale).

As one can see from Figure 7, there are no full energy peaks present. This is because the radiation being emitted are gamma-rays, and organic scintillators do not detect gamma-rays well, explaining the absence of the full energy peaks. What is detectable from the spectrums plotted in Figure 7 however is the compton edge and the backscatter peak and examples of both have been labeled. The area under each spectra from Figure 7 was determined with respect to the sources activity (Table 3). Source activities and the area under the curve were calculated using the following equations, where "μ" is the attenuation coefficient for each source [7] and “t” is the time since the source was born.

$$A = A_o e^{-\mu t} \tag{5}$$

$$Area\ Under\ Curve = Sum\ of\ total\ couts\ \times (\frac{A}{A_o}) \tag{6}$$

Table 3: Weighted area under spectra with respect to source's activities

Source	Gamma-Ray Energies (keV)	Source Activity (μCi)	Acquisition Time (s)	Area Under Curve (counts/Bq/s)
Cs-137	32, 662	9.77	90	65470
Co-57	122, 136.4	0.42	90	4008
Co-60	1173, 1333	0.60	90	59989
Cd-109	88	0.10	90	11056
Na-22	511, 1274.5	3.29	90	71425
Mn-54	834.3	0.47	90	81284

1 The gamma-ray energies for each source were found using NNDC [7].

From the table above it appears that the area does not change with respect to energy. Cs-137 and Na-22 do have larger areas but this is because the button source used were 10 μCi which is ten times as larger than the other initial activates. This lack of a change in area was as expected. Since organic scintillators do not detect the full energy peaks, all that was recorded in the spectrum was Compton scattered and backscattered radiation. These scatters are similar in every source, explaining the similar area distribution.

The spectrums for each source in Table 4 were obtained using the Preassembled NaI(TI) Detector. The peak positions and its uncertainties for the known gamma-ray energies were found using equations 1 and 2.

Table 4: Peak channel number for gamma-ray energies

Source	Gamma Energies (keV)	Channel Number of Peak	Peak Uncertainty
Cs-137	32, 662	19, 420	± 6, ± 29
Co-60	1173, 1333	738, 833	± 20, ± 23
Na-22	511, 1274	327, 780	± 20, ± 30
Co-57	122, 136.4	81, 91	± 6, ± 7
Cd-109	88	77	± 29

1 The gamma-ray energies for each source were found using NNDC [7].

The energy versus its peak channel number was plotted in Figure 8. A linear regression was conducted using the following equations (7 and 8), where "x" is energy, "y" is channel number, "A" is the y-intercept, and "B" is the slope of the regression line.

$$A = \frac{\sum y \sum x^2 - \sum x \sum xy}{N \sum x^2 - (\sum x)^2} \tag{7}$$

$$B = \frac{N \sum xy - \sum x \sum y}{N \sum x^2 - (\sum x)^2} \tag{8}$$

The resulting equation follows the form $y = Bx + A$. It was determined that the slope of the line was 0.60 ± 0.03 and the y-intercept was 9 ± 3 (equation and regression added to Figure 8).

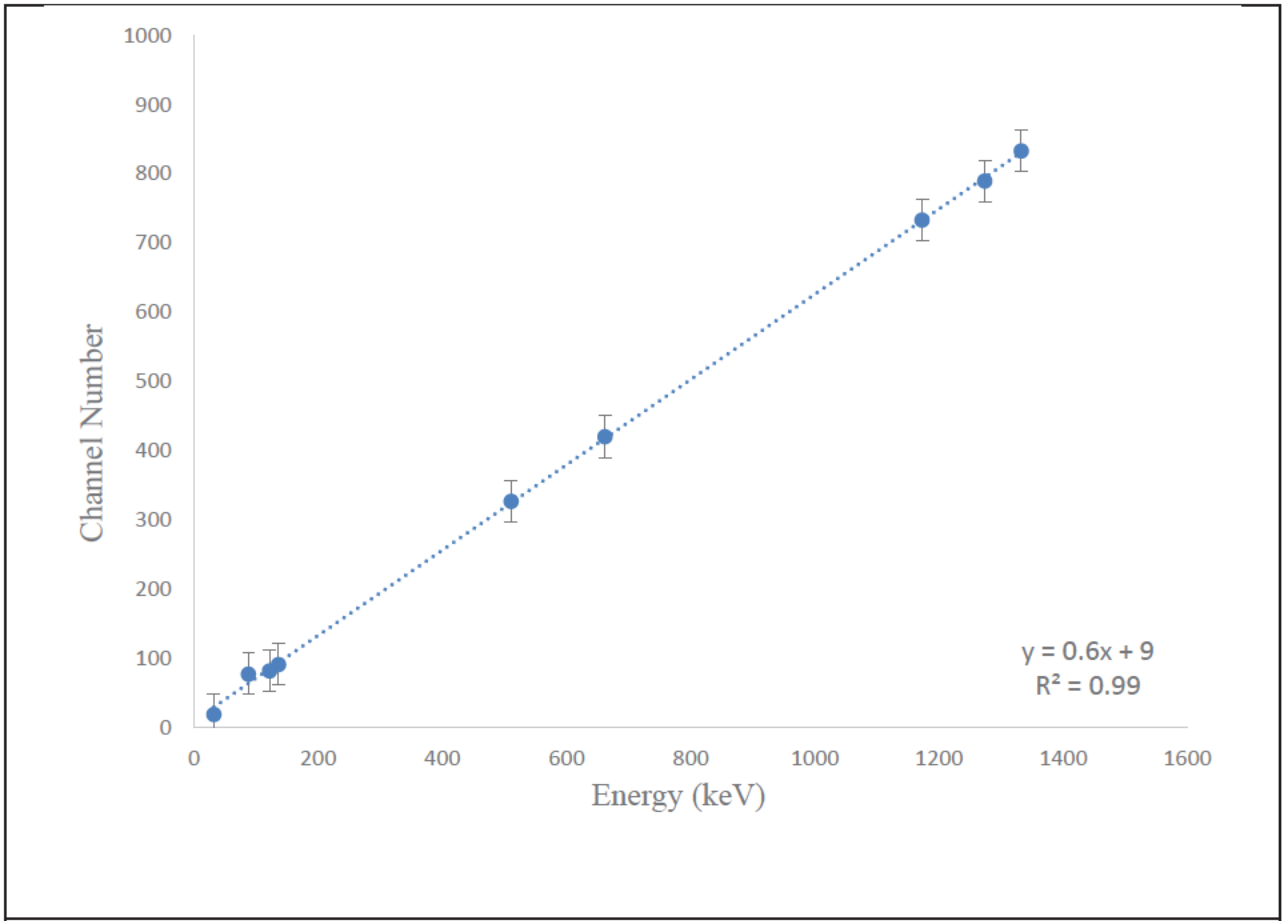

Figure 8: Gamma-ray energy versus their determined peak channel number. Regression line, correlation coefficient (R^2), and error bars included.

As one can see above, the linear regression is a very good fit to our data ($R^2 = 0.99$). This indicates that our NaI(Tl) detector being used to collect these gamma energies is proportional,

meaning it consistently reports gamma energies no matter if they are at low or high energies. This is how one would expect a properly functioning detector to perform. This linear correlation shows that the detector is properly detecting the emitted gamma-ray energies of each source.

For all of the sources in Table 4, the detector efficiency, peak efficiency and the energy resolution were calculated. These have been included in Table 5. The equations for the total detection efficiency, ratio, peak efficiency and energy resolution were determined using the following equations.

$$Total\ Detection\ Efficiency = intrinsic\ efficiency \times geometric\ efficiency \quad (9)$$

$$Ratio = \frac{Counts\ in\ Energy\ Peak}{Total\ Counts} \quad (10)$$

$$Peak\ Efficiency = Total\ Efficiency\ \times Ratio \quad (11)$$

$$Energy\ Resolution = \frac{2.36\sigma}{E_\gamma} \quad (12)$$

Table 5: Gamma-ray energy detection efficiency and energy resolution

Source	Gamma Energies (keV)	Total Detector Efficiency (%)	Peak Efficiency (%)	Ratio	Energy Resolution
Cs-137	32	10.1 ± 0.9	0.8 ± 0.07	0.078 ± 0.015	46 ± 4
	662	7.7 ± 0.7	1.8 ± 0.17	0.24 ± 0.04	10.3 ± 0.9
Co-60	1173	6.4 ± 0.6	0.17 ± 0.016	0.020 ± 0.005	3.9 ± 0.3
	1333	6.1 ± 0.6	0.14 ± 0.013	0.023 ± 0.005	4.1 ± 0.3
Na-22	511	8.3 ± 0.8	2.3 ± 0.20	0.27 ± 0.05	9.4 ± 0.8
	1274	6.2 ± 0.5	0.18 ± 0.15	0.021 ± 0.004	5.5 ± 0.5
Co-57	122	10.1 ± 0.9	2.55 ± 0.23	0.25 ± 0.005	12.6 ± 1.1
	136.4	10.1 ± 0.9	0.21 ± 0.19	0.021 ± 0.003	1.7 ± 0.2
Cd-109	88	10.1 ± 0.9	4.8 ± 0.4	0.48 ± 0.09	77 ± 7

1 The gamma-ray energies for each source were found using NNDC [7]

As one can see the total detection efficiency decreases as the gamma energy recorded increased. This trend continuous with both the ratio and the peak efficiency. For the energy resolution for each peak, the values remained small (12 or below) for all gamma energies except the two smallest energies (32 keV and 88 keV). For these two energies, the resolution was determined to be a very high value which indicates a lower resolution. This means these energy peaks were

broader. This could be due to the act that they are so low they begin to intertwine with lower energy background counts. This combination of desired and undesired peaks could have created a broader energy peak explaining the higher energy resolutions.

A background count was conducted for 15 minutes with all of the sources in the laboratory locked away. The background spectrum has been plotted in Figure 9. Notice that this time, unlike previous plots with the x-axis being channel numbers, this time the x-axis was converted to energy using the known relationship found in Figure 8.

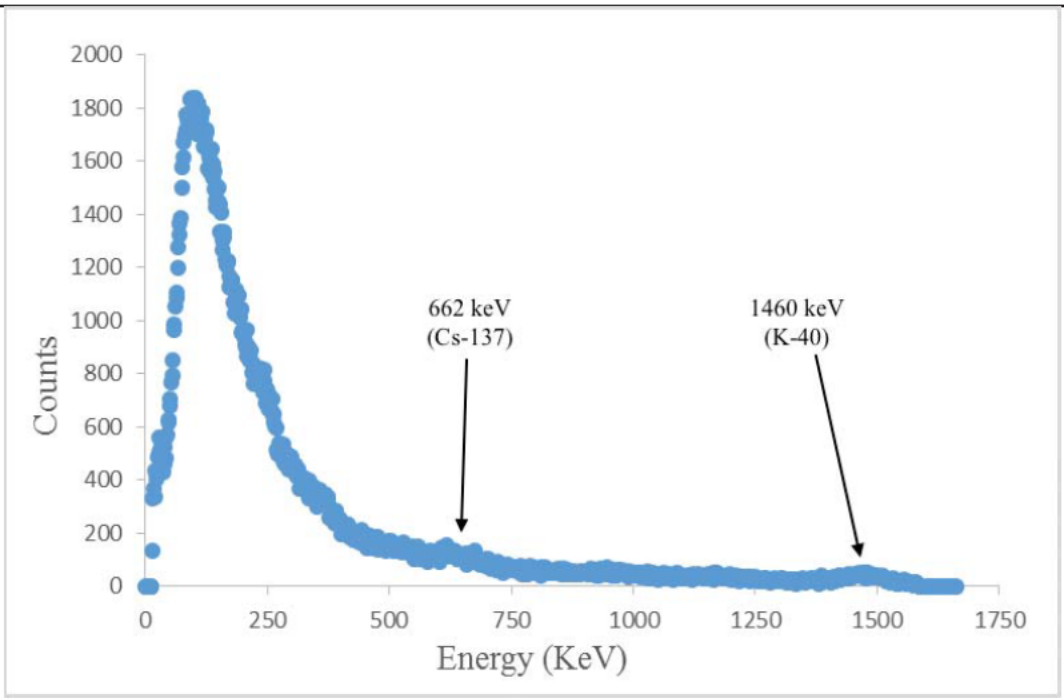

Figure 9: Background spectrum for NaI(Tl) detector. 662 keV and 1460 keV peaks identified from Cs-137 and K-40 [7].

The two peaks observed were attributed to Cs-137 (662 keV) and K-40 (1460 keV). The Cs-137 gamma-ray is expected as it is a typical in background spectrums because it is very common in materials, especially in a laboratory setting. The gamma-ray from K-40 is due to the fact that Potassium is present in the NaI(Tl) detector [6]. The high count peak at low energy is a combination of low energy gamma rays that are always present on Earth. They cannot be distinguished to specific elements due to the low resolution of the detector.

The Cs-137 differential pulse height spectrum was plotted along with the integral pulse height spectrum in Figure 10.

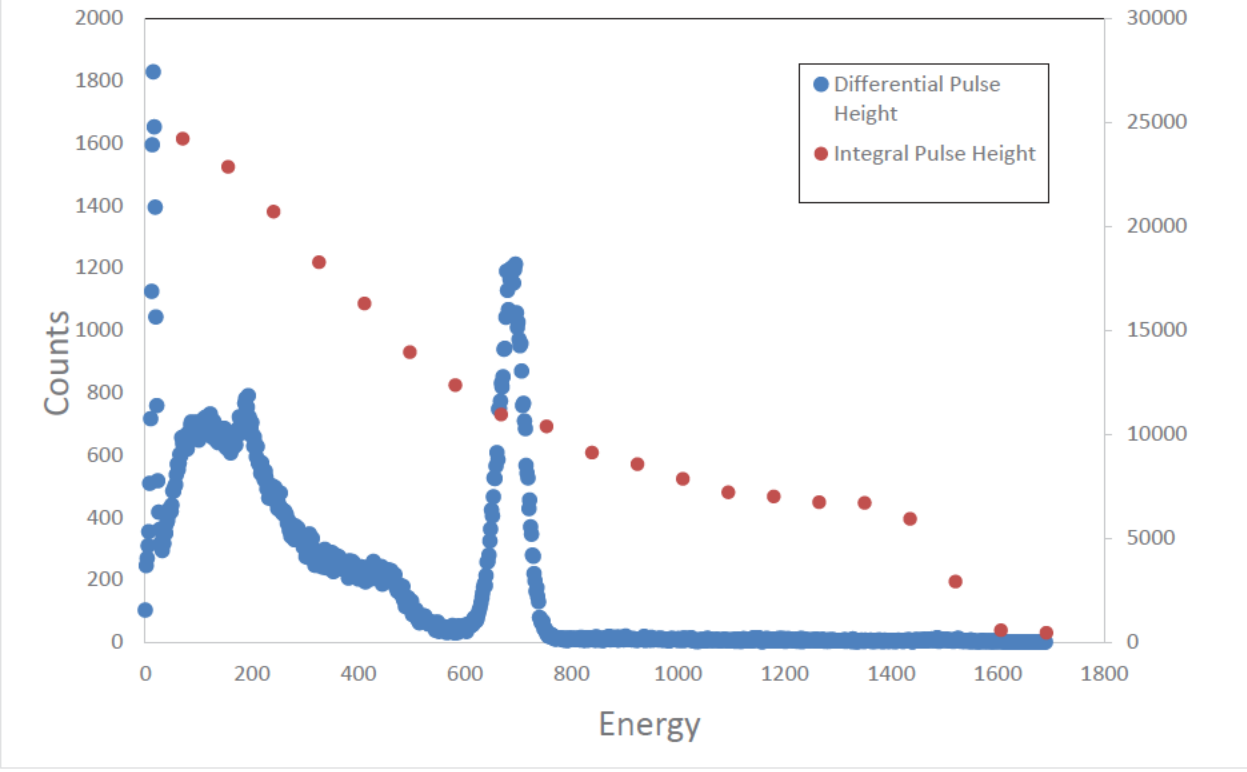

Figure 10: Cs-137 differential pulse height spectrum compared to the integral pulse height spectrum. (Note the major and minor axis are both counts but the major axis (left) correlates to the differential spectrum and the minor axis (right) correlates to the integral spectrum.

The data was unable to be plotted correctly due to possible miscounts for the integral pulse heights. Although Figure 10 does no show the integral and differential pulse spectrums in agreement, the overall shape of the two spectrums is as expected. To further analyze this relationship between the two, more spectrums for the integral pulse height would need to be conducted.

5. Conclusion (10%)

After analyzing the collected data for the spectrums recorded, the expected trends were seen for both the inorganic NaI(Tl) detector and the organic scintillation detector used. The first NaI(Tl) detector used was found to possess a linear relationship between applied voltage and outputted voltage which was as expected. This liner regression was used to determine the gain of the PMT. The gain was found to be $1.39 \pm 0.24 * 10^{-6}$. Although this did not exactly match the manufactures specification, the gain seems to be reasonable given the applied voltage to the

PMT throughout this experiment. The results from the investigation of the changes in shaping time with and without the preamplifier provided further evidence to for the preamplifier's importance. Without it, noise is more likely to make it to the amplifier which can result in unexpected peak outputs which could drastically effect further data analysis. The analysis of the organic scintillator provided spectrums which were exactly as expected. The organic scintillation detectors cannot detect gamma-rays which is why there was a clear absence of the gamma-ray energy peaks in Figure 7. Although there were no full energy peaks, there still was the presence of the lower energy compton scatters and backscatters detected. The last preassembled NaI(Tl) detector allowed for further analysis of gamma ray spectroscopy. The known gamma-rays emitted for each source used in the experiment, allowed for the correlation between the known energy and channel peak numbers to be determined. The strong linear fit calculated ($R^2 = 0.99$) allowed for the accurate conversation between channel numbers to energy. This made identification of other gamma-rays detected on the energy spectrum possible even when the sources of the peaks were unknown, as was conducted on the background spectrum.

Overall, the data collected was done with minimal error. Other than obtaining detectors with a better energy resolution, the only thing that could have been done to improve these experiments would be to conduct multiple spectrums opposed to just one, to ensure the most accurate spectrum is being investigated.

6. References

1. Grupen, C., & Shwartz, B. (2008). *Particle detectors* (Vol. 26). Cambridge university press. p. 126
2. Gardner, R. P., & Ely, R. L. (1967). *Radioisotope measurement applications in engineering*. Reinhold Publ. p. 90
3. Tsoulfanidis, N. (2013). *Measurement and detection of radiation*. CRC press. p. 195-213
4. Delaney, C. F., & Finch, E. C. (1992). *Radiation detectors*. Clarendon Press. p. 114
5. Knoll, G. F. (1979). *Radiation detection and measurement*. John Wiley & Sons. p. 272
6. K.K., H.P. *Photomultiplier tube assembly H6533.* [cited 2016 April 20]; Available from: http://www.hamamatsu.com/us/en/product/alpha/P/3002/H6533/index.html.
7. National Nuclear Data Center: p. www.nndc.bnl.gov.